

Chapter 4

Calcium Binding Behavior of α -Synuclein's C-terminal Tail

4.1 ABSTRACT

A feature of Parkinson's disease is the presence of fibrillar protein deposits composed mostly of α -synuclein and calcium ions in the *substantia nigra* region of the brain. Although α -synuclein is natively unfolded, the N-terminal region of the protein is highly helical in the presence of membrane mimics, such as acidic phospholipid vesicles. It has been postulated that calcium ions bind to the acidic C-terminal tail of α -synuclein. We have incorporated three tryptophan variants (W101, W125, and W136) in that region and investigated the interactions between the phospholipid vesicles and calcium ions by steady-state and time-resolved fluorescence spectroscopy. We have also prepared seven mutants (W94/Y113(NO₂), W94/Y125(NO₂), W94/Y136(NO₂), W101/Y74(NO₂), W101/Y125(NO₂), W101/Y136(NO₂), and W125/Y136(NO₂)), and probed the change of distance distributions in the presence of calcium ions by fluorescent energy transfer and electron transfer using tryptophan as the donor and 3-nitrotyrosine as the acceptor. The results suggest that the C-terminal tail is capable of binding to two calcium ions in solution, while one of the calcium binding regions weakens when the α -synuclein mutants are placed in phospholipid vesicles.

4.2 INTRODUCTION

α -Syn is a 140-residue protein with unknown function.¹ The protein is commonly classified into three regions. The C-terminal domain consists of residues 96–140. This region has been noted by the large number of acidic residues (10 Glus and 5 Asps) and its ability to bind to calcium ions,^{2,3} copper ions,⁴ microtubule-associated proteins 1B,⁵ and polyamines.⁶

The C-terminal domain has been demonstrated to be multi-functional and is strongly related to the aggregation properties of α -syn. It is responsible for the protein's stability at high temperature,⁷ acts as a solubilizing domain for chaperone function,⁸⁻¹¹ and prevents aggregation. It has been previously shown that α -syn with a truncated C-terminal tail has a tendency to aggregate at a faster rate.¹²⁻¹⁴ Post-translational modifications of some C-terminal tail residues can also change the susceptibility for α -syn to aggregate.^{15,16} Although the C-terminal tail is responsible for mediating aggregation, it is structurally found on the surface of the fibrils, rather than being incorporated into the core.¹⁷⁻¹⁹

A high concentration of calcium ions and α -syn are two important factors for the initiation of PD.²⁰ In addition, aging is an important risk factor for PD. The aging process, such as the neurodegeneration observed in PD, has been associated with oxidative stress.²¹ This oxidative stress has been linked to calcium dysregulation, which can possibly affect cellular processes through an influx of calcium ions, thus increasing the internal calcium ion concentration.²²⁻²⁵

In the presence of membrane mimics, such as SDS micelles and acidic SUVs, the N-terminal portion of α -syn becomes highly helical, while the C-terminal tail has been shown to remain largely unstructured. De Laureto et al. have previously studied the influence of calcium ions on the structure of the C-terminal tail α -syn by proteolysis.²⁶ They have observed that, in the presence of calcium ions, thermolysin, proteinase K, and Glu-specific V8-protease can degrade α -syn into various small fragments in solution. However, in the presence of 10 mM SDS micelles, fragmentation sites were only identified at the C-terminal end of residues 111, 113, and 123. This result illustrates that the C-terminal tail can be made rigid by the presence of membrane mimics.

Separately, Tamamizu-Kato et al. introduced a pyrene fluorophore onto residue 125 of α -syn.²⁰ They have observed an increase in the band III fluorescence emission upon addition of calcium ions, thus suggesting that there is increased interaction between residue 125 and the membrane. It has been proposed that the N-terminal domain and lipids first interact with each other, then the C-terminal tail is associated with the lipid bilayer triggered by the addition of calcium ions.

In this study, we first investigated whether the C-terminal tail of α -syn binds to the surface of SUVs in the presence of calcium ions by steady-state and time-resolved fluorescence spectroscopy. Single Trp mutants (W101, W125, and W136) were employed as a fluorescent probe and represent different regions of the C-terminal tail. Phospholipids containing heavy-atom (Br) and energy-transfer (dinitrophenol) quenchers were incorporated into SUVs to determine the position of the Trp mutants in the presence of calcium ions.²⁷

Time-resolved fluorescent energy-transfer (FET) was then used to probe the structural changes in the C-terminal tail of α -syn in solution and acidic SUVs upon the addition of calcium ions. Since fluorescent donor-acceptor (D-A) distance is inversely proportional to the FET rate,²⁸ probability distribution of D-A distances can be extracted.^{27,29-33} Seven α -syn mutants have been expressed with D-A placed along various parts of the C-terminal tail to further probe behavior in the presence of SUVs and calcium ions.

The fluorescent amino acid tryptophan (Trp) has been chosen as the fluorescent donor for this study. A chemically modified tyrosine, 3-nitrotyrosine [Tyr(NO₂)], was utilized as an energy acceptor. The Förster distance for this D-A pair is 26 Å.³⁴ The N-terminal and C-terminal interface was probed by Y74(NO₂)/W101, W94/Y113(NO₂). The whole C-terminal tail was characterized by W94/Y125(NO₂), W94/Y136(NO₂), W101/Y125(NO₂), W101/Y136(NO₂). The extreme C-terminal end of the protein was studied by W125/Y136(NO₂).

It is also our interest to study the effect of calcium ions on the tertiary contact formation of the C-terminal tail of α -syn. Photoinduced electron transfer (ET) from the triplet excited state of tryptophan to 3-nitrotyrosine can be measured to determine the contact formation in various environments.^{35,36} Time-resolved absorption experiments were employed to study the mutants listed above. Tryptophan is excited by a laser pulse to generate a singlet excited state (¹W*). This singlet excited state can proceed through intersystem crossing to create a Trp triplet excited state (³W*). This triplet excited state can then be quenched by 3-nitrotyrosine if it is in proximity of the ³W*.

4.3 METHODS

Protein Expression, Modification, and Purification.

The plasmid of wild-type α -syn was provided by M. Goedert³⁷. For the single Trp studies, site-directed mutagenesis was employed to introduce Trp in five different sites (W4, W94, W101, W125, and W136). For studies involving Trp as a donor and Tyr as an acceptor, a single Trp was mutated into the sequence (W101, W125, and W136). Extra Tyrs were also mutated away into Phes. One Tyr was introduced or remained in the sequence as the nitration site.

Expression, modification, purification, and nitration protocols have been adopted from Chapter 1. The purity of protein samples were evaluated by SDS-PAGE on a Pharmacia Phastsystem (Amersham Biosciences) and mass spectrometry (California Institute of Technology Protein/Peptide Microanalytical Laboratory).

SUVs Fabrication.

Quencher-free SUVs were made with 1:1 molar mixture of two lipids, namely 1-palmitoyl-2-oleoyl-*sn*-glycero-3-phosphocholine (POPC) and 1-palmitoyl-2-oleoyl-*sn*-glycero-3-phosphate (POPA). For SUVs containing brominated lipids, 1-palmitoyl-2-stearoyl(6,7-dibromo)-*sn*-glycero-3-phosphocholine (DiBr) was chosen, with a 1:2:1 molar ratio of POPC:POPA:DiBr. The distance between the polar end of the lipid and the bromine atoms is 9 Å. On the other hand, the lipid labeled with an energy-transfer quencher, N-dinitrophenyl phosphatidylethanolamine (DNP), was

used to fabricate SUVs with a quencher installed at the head group. A molar ratio of 4:5:1 POPC:POPA:DNP was achieved in these SUVs.

SUVs were fabricated following protocol in Chapter 1. Lipid solutions were dried under a stream of Ar for 5 min and under vacuum for 30 min. Dried lipids were suspended in 10 mM HEPES (pH 7.4) at a concentration of 5 mg/mL. The lipid solution was then sonicated by a Branson ultrasonicator microtip (Plainview, NJ) for 30 min at 50% duty cycle (200 W). The sonicated SUVs were then diluted with HEPES to yield a final concentration of 2 mg/mL and equilibrated at room temperature overnight. However, for ET experiments, lipid solutions were sonicated and equilibrated at 10 mg/mL. The SUV solution was then centrifuged at $10,000 \times g$ for 10 min to remove titanium dust and particulates. Freshly prepared SUVs were used for all experiments.

Sample Preparation and Steady-state Fluorescence Experiments.

Sample preparation and data processing procedures for fluorescence studies have been described in Chapter 1, except all protein samples were exchanged into 10 mM HEPES (pH 7.4). All experimental samples contained 5 μ M protein with 1.4 mg/mL SUVs. However, for ET experiments, 15 μ M protein with 4.2 mg/mL SUVs was used. Calcium ions were supplied by CaCl_2 .

Time-resolved Absorption Experiment.

Experimental samples were deoxygenated using the same protocol as described above.³⁶ N_2O , a solvated-electron scavenger, was equilibrated with the

sample. $^3W^*$ was generated by exciting the sample with the second harmonic (290 nm) of a nanosecond Nd:YAG pumped optical parametric oscillator laser (Spectra-Physics). An Ar-ion laser (457.9 nm) was used as a source of probe light. The sensitivity of our measurements was improved by passing the probe light through the sample multiple times, thus increasing the path length from 1 to 7 cm. Transient absorption kinetics were detected by a photodiode and recorded using an 8-bit, 500-MHz digital oscilloscope (LeCroy 9354A).

For data analysis, the traces were transformed to absorbance changes [$-\log_{10}(I_{\text{sample}}/I_{\text{reference}})$]. They were then logarithmically compressed (100 points per decade) and normalized [$OD(t) - OD(t_{\infty})/OD(t_0) - OD(t_{\infty})$]. The adjusted traces were then fitted with NNLS.

4.4 DISCUSSIONS AND CONCLUSIONS.

Calcium Ion Titration Curve.

To determine the amount of calcium ions needed to induce structural formation, steady-state fluorescence spectra of single Trp mutants at different concentrations of calcium ions were taken. Acquired Trp fluorescence is an excellent probe in determining Trp microenvironment³⁸⁻⁴¹. It has been demonstrated that a smaller Stokes shift and a higher quantum yield can be observed when the Trp is inserted into the lipid bilayer. Therefore, the integrated intensities between 325 and 500 nm can reveal whether the Trps are inserted into the lipid bilayer at various calcium ion concentrations.

Figure 4.1a shows the integrated intensities of the three Trps (Trp101, Trp125, and Trp136) and the tryptophan analog, NATA, in the presence of various calcium ion concentrations and SUVs. It is demonstrated that the integrated intensities remain relatively unchanged for W125, W136, and NATA between 0 - 1 mM of calcium ions. On the other hand, a steady increase of fluorescence intensity was observed as more calcium ions were added to the W101 sample, with the intensity reaching a steady maximum around 1 mM. This experiment implies that only Trp101 became more closely associated with the lipid bilayer when 1 mM calcium ions were added in the presence of SUVs. Adding more calcium ions yielded no changes to all three mutants studied, along with NATA (data not shown).

Similar calcium ion titration experiments were performed in the presence of SUVs. **Figure 4.1b** shows that the integrated fluorescence intensities for all three Trps and NATA remained largely unchanged when 1 mM calcium ions were added. Although this experiment shows that the Trps will remain in similar environments when calcium ions are added in the presence of SUVs, it is unclear whether the C-terminal tail binds to any calcium ions.

Time-resolved Fluorescent Lifetime Studies.

We have previously employed DiBr-containing SUVs to characterize Trp positions when the protein is folded into the lipid bilayer^{37,39,42,43}. **Figure 4.2** shows the NNLS-fitted time-resolved fluorescent decay of the three Trps studied. Similar lifetimes of NATA have been observed in solution (blue traces), 1:1 POPC:POPA SUVs (red traces), and DiBr SUVs (green traces) in the presence (dotted traces) or

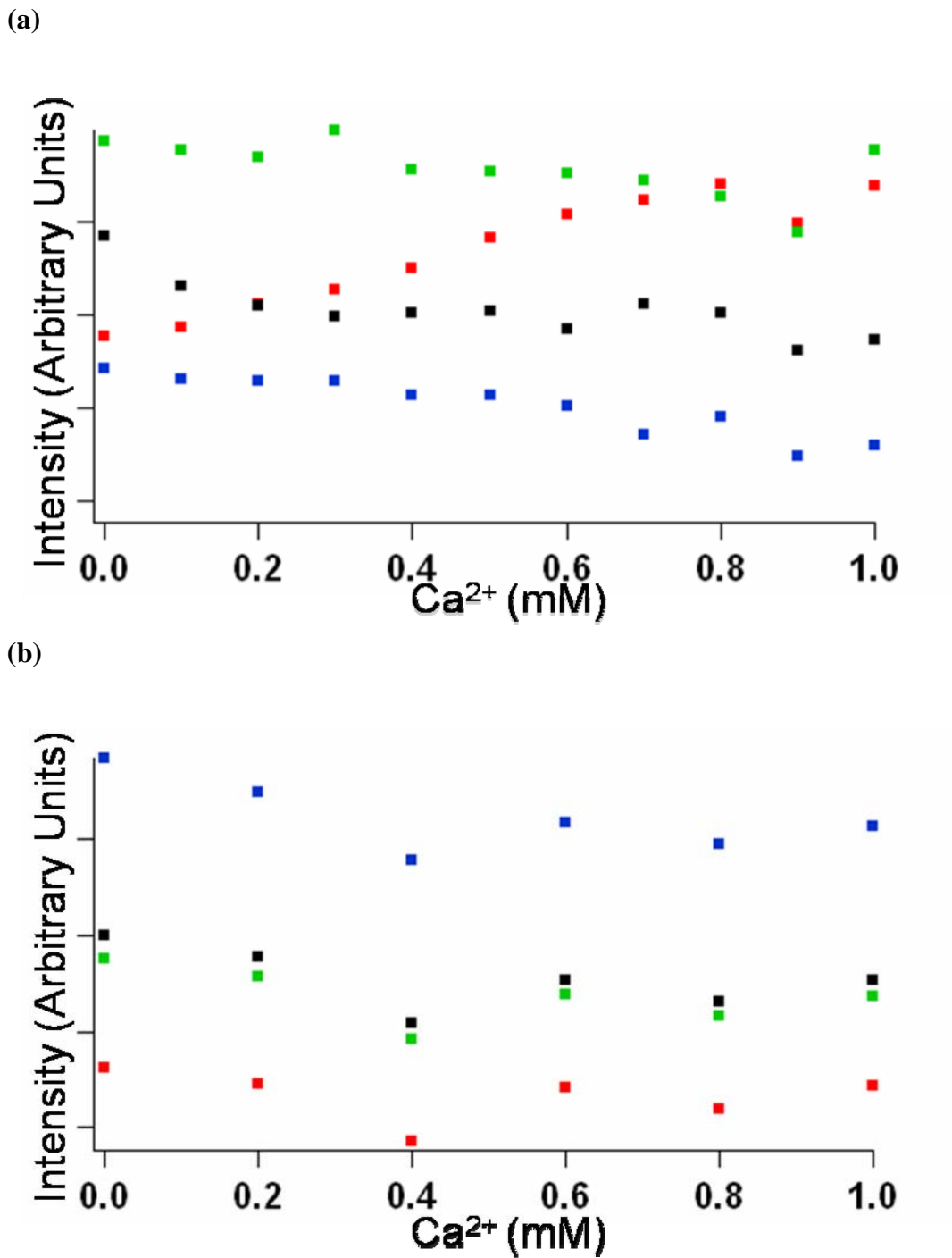


Figure 4.1. Integrated fluorescence intensity between 325 nm and 500 nm of W101 (red), W125 (green), W136 (blue), and NATA (black) in various concentrations of Ca^{2+} and in the (a) absence or (b) presence of SUVs

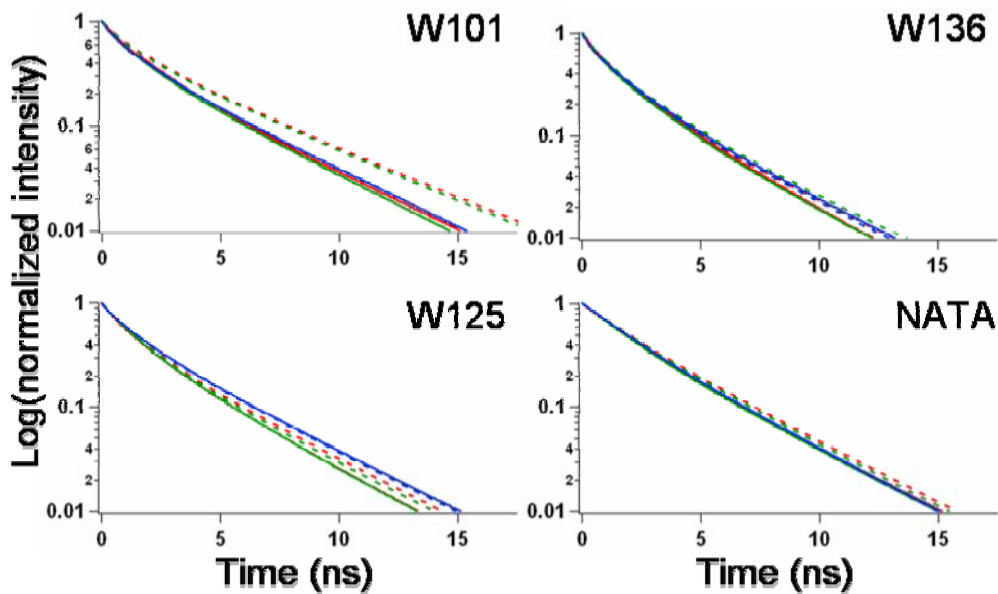


Figure 4.2. Time-resolved fluorescent decay of α -syn mutants W101 (top-left panel), W125 (bottom-left panel), W136 (top-right panel), and NATA (bottom-right panel) in the presence of HEPES (blue solid line), HEPES and Ca^{2+} (blue dotted line), 6,7-DiBr SUV (green solid line), DiBr SUV and Ca^{2+} (green dotted line), 1:1 POPC:POPA SUV (red solid line), and 1:1 POPC:POPA SUV and Ca^{2+} (red dotted line)

absence (solid traces) of calcium ions. W125 and W136 show time-resolved fluorescent decay comparable to NATA in the various environments described above.

Although W101 shows similar time-resolved fluorescent lifetimes in the absence of calcium ions, there is an increase in lifetimes when calcium ions are added into samples containing 1:1 POPC:POPA SUVs. The extended fluorescent lifetimes indicate that the Trp has displayed a higher quantum yield, thus implying that the Trp is in a more hydrophobic environment, such as the lipid bilayer. This experimental result demonstrates that W101 is more associated with the membrane in the presence both SUVs and calcium ions, but not W125 and W136.

We have previously employed SUVs incorporated with heavy atom (Br) and energy transfer (dinitrophenol) quenchers to predict the specific location of Trps when α -syn is folded into the membrane.^{29,44} Again, we used the brominated lipid DiBr, where the quencher Br atoms are 9 Å away from the headgroup.⁴⁵ On the other hand, the dinitrophenol (DNP) has its quencher located on the lipid headgroup. By determining the amount of quenching of α -syn mutants in these quencher-containing SUVs, it is possible to elucidate how deep the C-terminal tail is inserted into the lipid bilayer in the presence of calcium ions.

As suggested by **Figure 4.2**, the fluorescent lifetimes for W101 are comparable when the α -syn mutant was placed in 1:1 POPC:POPA SUVs and DiBr SUVs. The lack of quenching by the brominated lipids implies that W101 was not inserted deeply into the membrane.

Previously we have also employed 10% DNP SUVs to investigate the position of these C-terminal mutants with respect to the surface of the vesicles.^{29,44} The time-

resolved fluorescent kinetic traces were fitted using NNLS method, with special attention paid to the ultra-fast lifetimes (< 0.1 ns) related to the energy transfer from Trp to the dinitrophenol group. In our previous study, we have demonstrated that none of the C-terminal mutants have this ultra-fast lifetime component. However, based on the amplitude of the fast decay component ($\sim 1 \times 10^{-9} \text{ s}^{-1}$), Trp101 (38%) displays the highest population, followed by W136 (14%) then W125 (2%).

In this study, we focus on the populations of the fast lifetime components ($> 1 \times 10^{-9} \text{ s}^{-1}$) of the Trp mutants in the presence of calcium ions and 10% DNP SUVs. If an increase of these fast lifetime components is observed, it can imply that calcium ions are mediating membrane association with the C-terminal tail region. **Figure 4.3** shows that the change of amplitude for the fast lifetime components of NATA and W136 is minimal when calcium ions were introduced. This agrees with the time-resolved fluorescence data, suggesting that W136 does not become closely associated with the lipid bilayer upon the addition of calcium ions.

Among the three Trp C-terminal mutants studied, W101 demonstrates the highest increase in the fast lifetime population (25%), indicating that the region around W101 is associated with the surface of the membrane fairly closely, but not deeply inserted. This result is not surprising as the time-resolved fluorescence data has already suggested that W101 forms a closer contact with the lipid bilayer, while the lack of quenching in the time-resolved fluorescent lifetimes of Trp101 with DiBr SUVs shows that the Trp is not deeply inserted into the membrane.

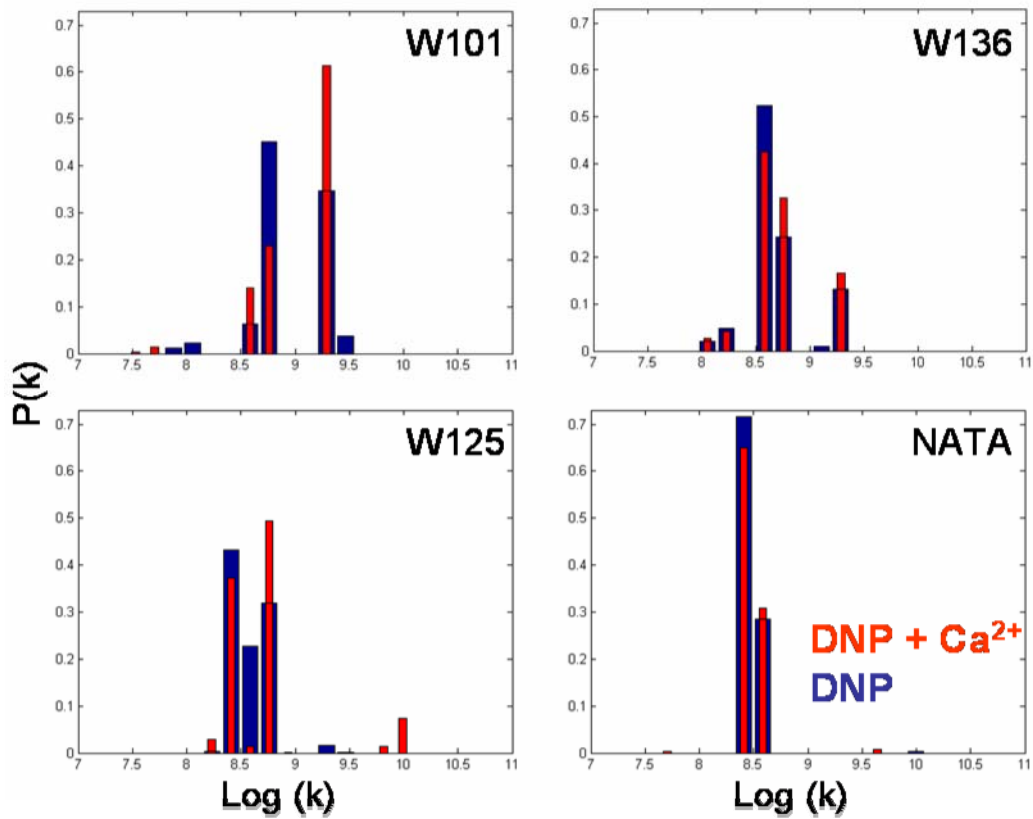


Figure 4.3. Distributions of tryptophan decay rate constants (k) for W101 (top left), W125 (bottom left), W136 (top right), and NATA (bottom right) α -syn mutants with 10 % DNP SUVs in the absence (blue) and presence (red) of Ca^{2+} (red)

What is interesting from this study is that W125 shows a modest increase of quenching (10 %) when calcium ions were added into the sample. A possible explanation is that the early segment of the C-terminal tail becomes closely associated with the lipid bilayer, mediated by the presence of the calcium ions. Therefore, W125 can be found closer to the membrane surface, although it is not directly associated with the membrane itself.

Time-resolved Anisotropy Studies.

The time-resolved fluorescent anisotropy decays for the three Trp-only mutants were carried out in the presence of 1:1 POPC:POPA SUVs with 1 mM of calcium ions (**Figure 4.4**). The anisotropy decays were fitted with biexponential decays. The rotation correlation times (θ) and anisotropies at time zero (r_0) were extrapolated to reveal the flexibility and the size of the Trps, thus providing information on how embedded the Trps are in different environments. These data were compared against the numbers obtained from Chapter 2 to determine the effect of calcium ions on the C-terminal mutants with respect to the membrane.

The three C-terminal Trp mutants display a dramatic increase of r_0 in the presence of calcium ions, with W101 ($r_0 = 0.11$ in SUVs and 0.23 in SUVs + Ca^{2+}) and W136 ($r_0 = 0.10$ in SUVs and 0.22 in SUVs + Ca^{2+}) doubling their r_0 values. On the other hand, W125 only shows a modest increase of r_0 value from 0.10 to 0.17 when calcium ions were added.

In addition, **Figure 4.4** exhibits a sharp decrease of r -value within 0.2 ns. Contrary to the anisotropy decay curves shown in **Figure 2.8**, the r -values of the C-

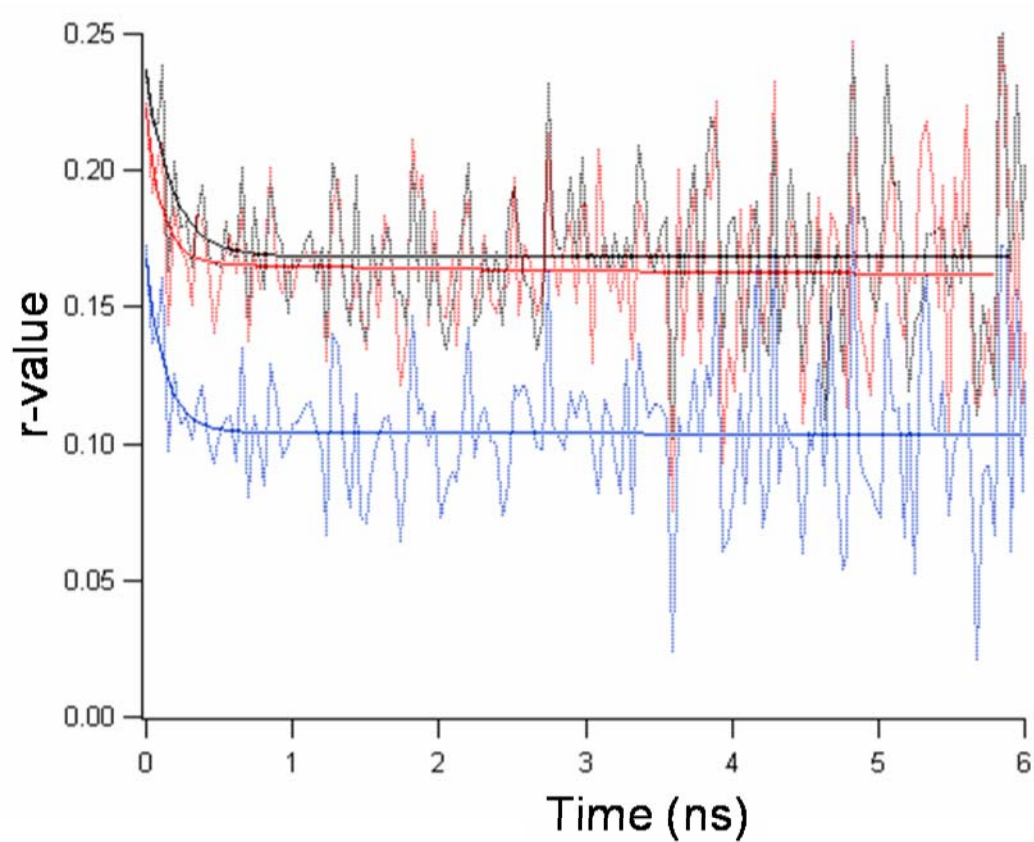


Figure 4.4. Time-resolved anisotropy decays for α -syn mutants W101 (red), W125 (blue), and W136 (black) in 1:1 POPC:POPA SUVs in 1 mM Ca^{2+}

terminal Trp mutants do not go to zero in the presence of calcium ions. It is possible to conclude that the all Trps in the C-terminal tail are now in a more rigid environment, caused by the calcium ions. Among the three C-terminal mutants, it is not surprising to note that W101 becomes more rigid with calcium ions. It has been shown previously that calcium ions mediate closer interaction between W101 and the membrane. However, W136 also demonstrates some degree of rigidity in the presence of calcium ions, so that region could possibly serve as a calcium binding region.

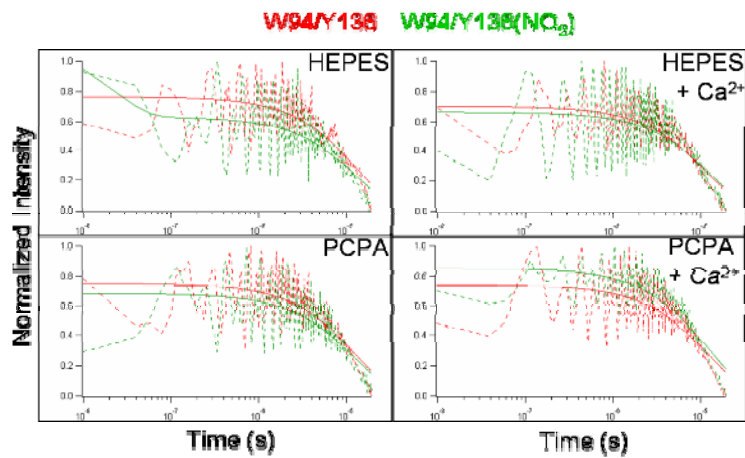
Electron Transfer Study.

The electron transfer rates between $^3\text{Trp}^*$ and Tyr(NO₂) for the seven D-A pairs in solution and SUVs have been measured, either in the presence or the absence of calcium ions. The ET rates (**Table 4.1** and **Figure 4.5–4.7**) have been fitted using the NNLS protocol. If α -syn mutants are placed in an environment where Trp and Tyr(NO₂) become close in contact, the ET rate will decrease significantly. In addition, the ET rate is also dependent on the average D-A distances and the stiffness of the polypeptide chain joining D-A.³⁶ Therefore, the ET rates can also shed light on whether the various changes in the mutants' surroundings can cause the C-terminal sequence to stiffen.

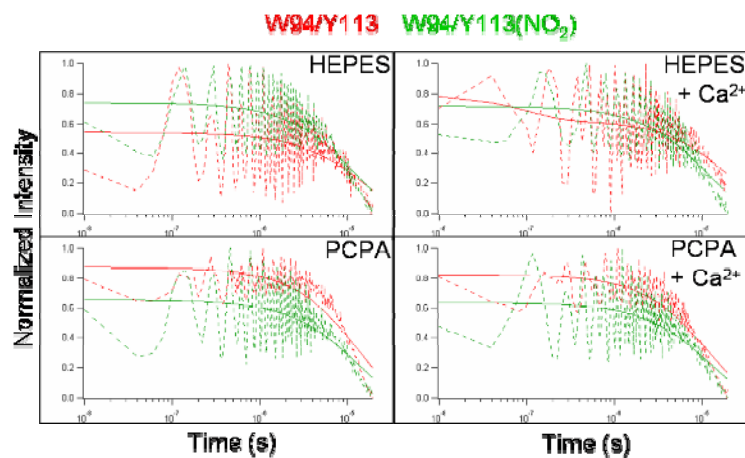
In addition to measuring the ET rates for the seven D-A mutants, the rates for their non-nitrated counterparts were also investigated as a control experiment. As **Table 1** suggests, all seven nitrated mutants demonstrate similar ET rates compared to their controls, regardless of which environments (buffer, buffer with calcium ions,

Mutant	Environment	τ (μ s)	Mutant	Environment	τ (μ s)
W94/Y125	HEPES	20	W94/Y125(NO ₂)	HEPES	21
	HEPES + Ca ²⁺	20		HEPES + Ca ²⁺	14
	SUV	20		SUV	14
	SUV + Ca ²⁺	17		SUV + Ca ²⁺	17
W94/Y136	HEPES	20	W94/Y136(NO ₂)	HEPES	20
	HEPES + Ca ²⁺	18		HEPES + Ca ²⁺	20
	SUV	19		SUV	19
	SUV + Ca ²⁺	18		SUV + Ca ²⁺	18
W94/Y113	HEPES	22	W94/Y113(NO ₂)	HEPES	18
	HEPES + Ca ²⁺	33		HEPES + Ca ²⁺	17
	SUV	20		SUV	18
	SUV + Ca ²⁺	18		SUV + Ca ²⁺	18
W101/Y125	HEPES	25	W101/Y125(NO ₂)	HEPES	18
	HEPES + Ca ²⁺	16		HEPES + Ca ²⁺	17
	SUV	20		SUV	18
	SUV + Ca ²⁺	16		SUV + Ca ²⁺	17
W101/Y136	HEPES	16	W101/Y136(NO ₂)	HEPES	15
	HEPES + Ca ²⁺	19		HEPES + Ca ²⁺	15
	SUV	17		SUV	15
	SUV + Ca ²⁺	19		SUV + Ca ²⁺	16
W101/Y74	HEPES	21	W101/Y74(NO ₂)	HEPES	17
	HEPES + Ca ²⁺	16		HEPES + Ca ²⁺	17
	SUV	18		SUV	20
	SUV + Ca ²⁺	17		SUV + Ca ²⁺	16
W125/Y136	HEPES	18	W125/Y136(NO ₂)	HEPES	16
	HEPES + Ca ²⁺	15		HEPES + Ca ²⁺	15
	SUV	16		SUV	18
	SUV + Ca ²⁺	16		SUV + Ca ²⁺	17

Table 4.1. The electron transfer rates (τ) of the α -syn mutants in the various environments

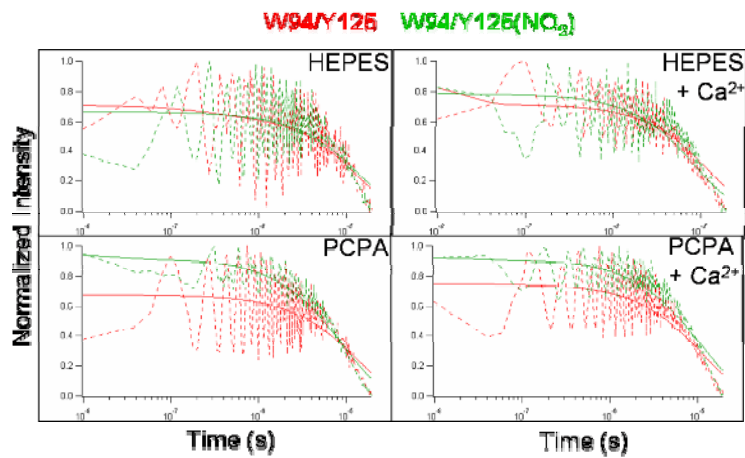


(a)

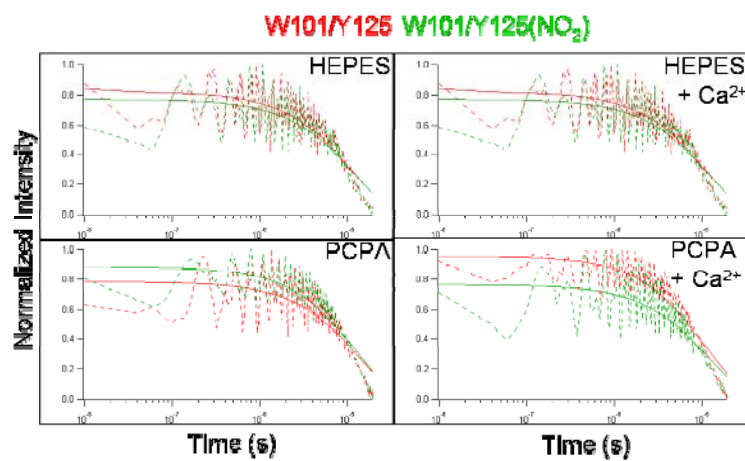


(b)

Figure 4.5. Electron transfer decay curves for (a) W94/Y136 (red) and W94/Y136(NO₂) (green) and (b) W94/Y113 (red) and W94/Y113(NO₂) (green) and in HEPES (top left), HEPES + Ca²⁺ (top right), 1:1 POPC:POPA SUVs (left bottom), and 1:1 POPC:POPA SUVs + Ca²⁺ (right bottom)



(a)



(b)

Figure 4.6. Electron transfer decay curves for (a) W94/Y125 (red) and W94/Y125(NO₂) (green) and (b) W101/Y125 (red) and W101/Y125(NO₂) (green) in HEPES (top left), HEPES + Ca²⁺ (top right), 1:1 POPC:POPA SUVs (left bottom), and 1:1 POPC:POPA SUVs + Ca²⁺ (right bottom)

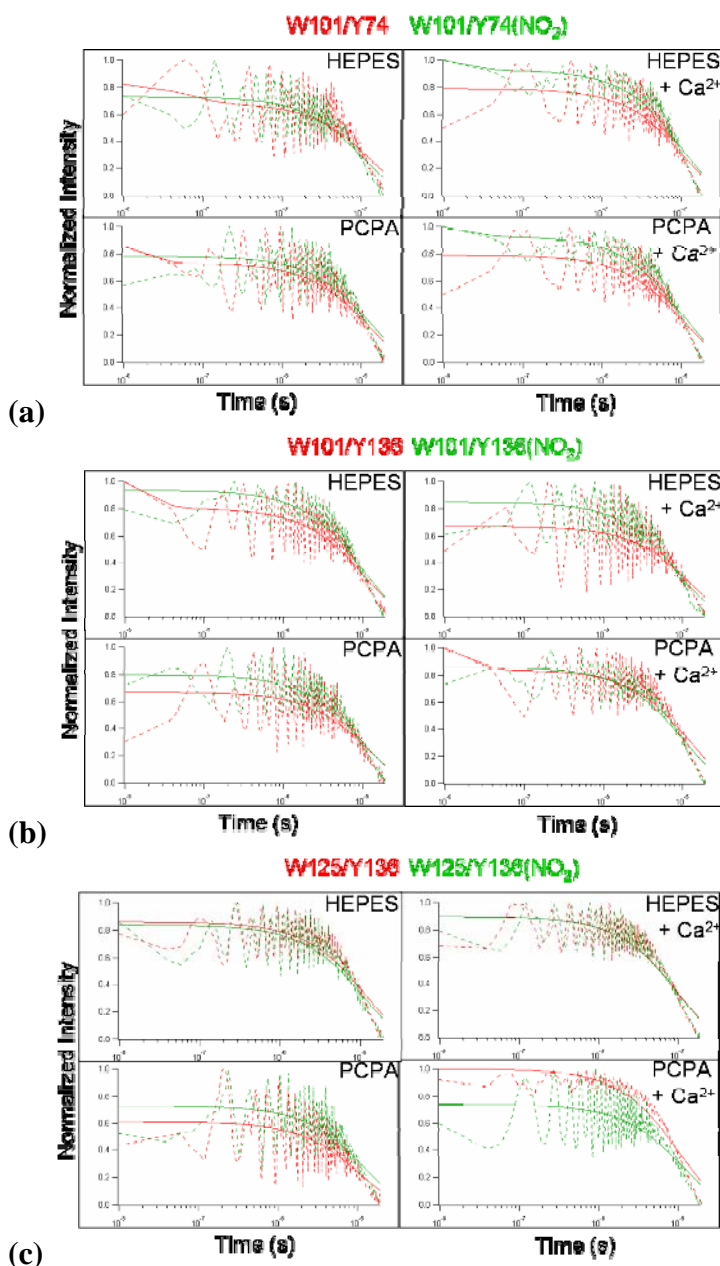
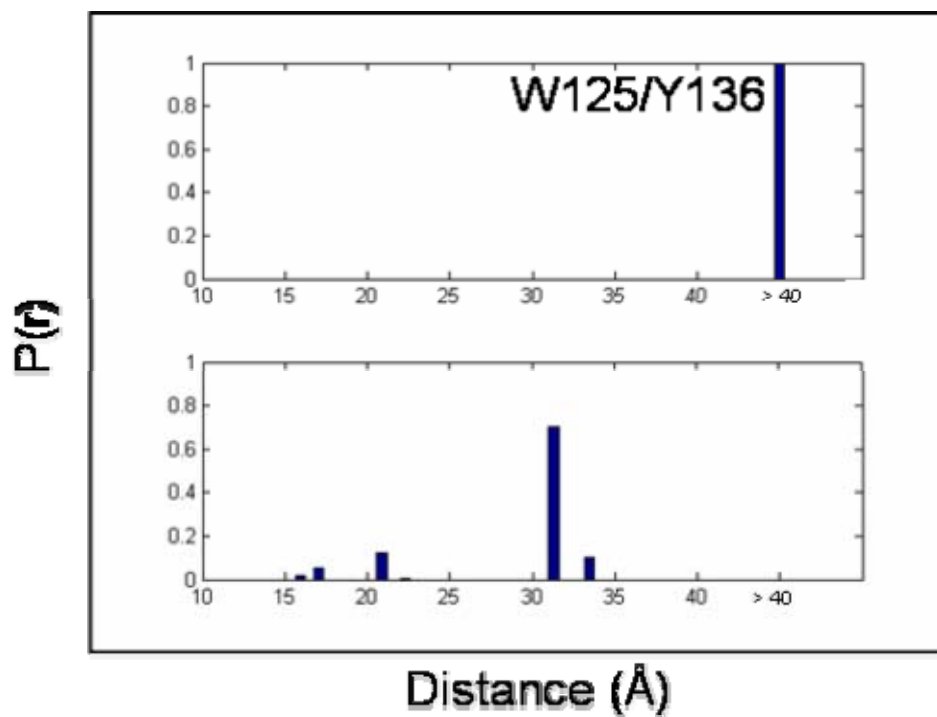


Figure 4.7 Electron transfer decay curves for (a) W101/Y74 (red) and W101/Y74(NO_2) (green), (b) W101/Y136 (red) and W101/Y136(NO_2) (green), and (c) W125/Y136 (red) and W125/Y136(NO_2) (green) in HEPES (top left), HEPES + Ca^{2+} (top right), 1:1 POPC:POPA SUVs (left bottom), and 1:1 POPC:POPA SUVs + Ca^{2+} (right bottom)

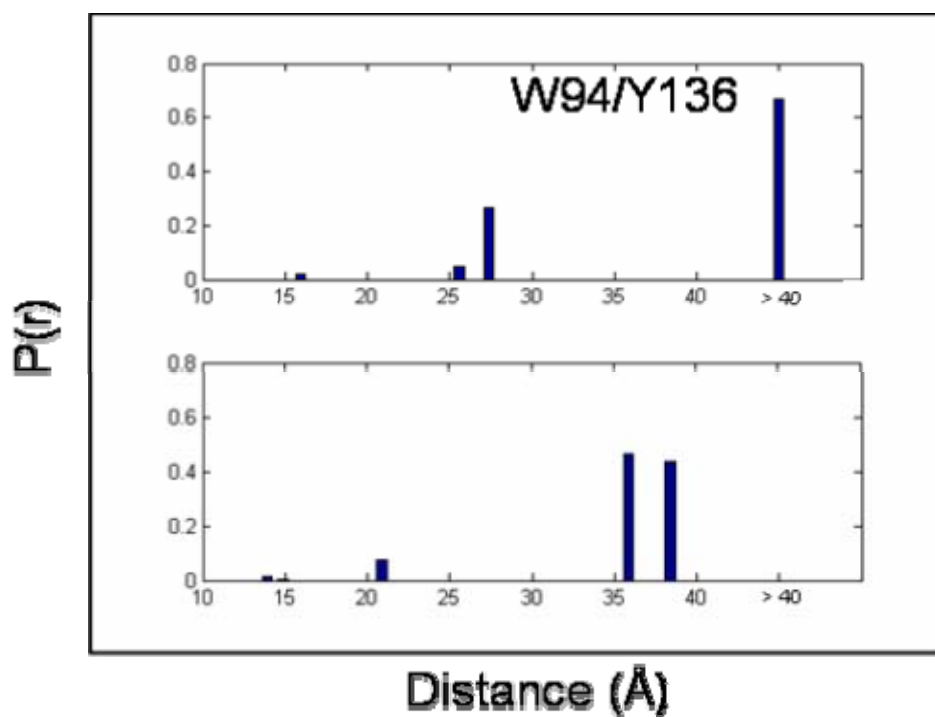
SUVs, and SUVs with calcium ions) these mutants were placed in. These experimental results imply that Trp and Tyr(NO₂) are not in close contact in any tested conditions. This phenomenon could be expected when calcium binding occurs, as the calcium ions preclude Trp and Tyr(NO₂) coming into close proximity. However, it comes as a surprise that ET between Trp and Tyr(NO₂) cannot be observed when these α -syn mutants were in solution-only environment. Lee et al. has previously shown that there are some predetermined structures when α -syn is in solution, even though it has been considered as natively unfolded.³⁶ Another potential cause of this phenomenon is the prevalence of acidic residues, as these negative charges repel each other, thus disallowing contact formation.

FET study.

Figure 4.8 and **Figure 4.9** show the distance distributions of four of the seven D-A α -syn mutants in solution in the presence/absence of calcium ions, extrapolated from time-resolved fluorescent energy transfer. In solution, W125/Y136(NO₂) mutant shows little quenching (decay curves not shown). However, with the addition of calcium ions, there is a small degree of quenching. The distance distribution of fitted data shows that there is formation of a population with smaller distance populations (~ 31 Å), implying there is a possible calcium binding region between residue 125 and 136. This phenomenon is also supported by the distributions obtained in W94/Y136(NO₂). For W94/Y136(NO₂), there is a shift from long distance distributions (> 40 Å) to shorter distance distributions (~ 37 Å) upon the addition of calcium ions.

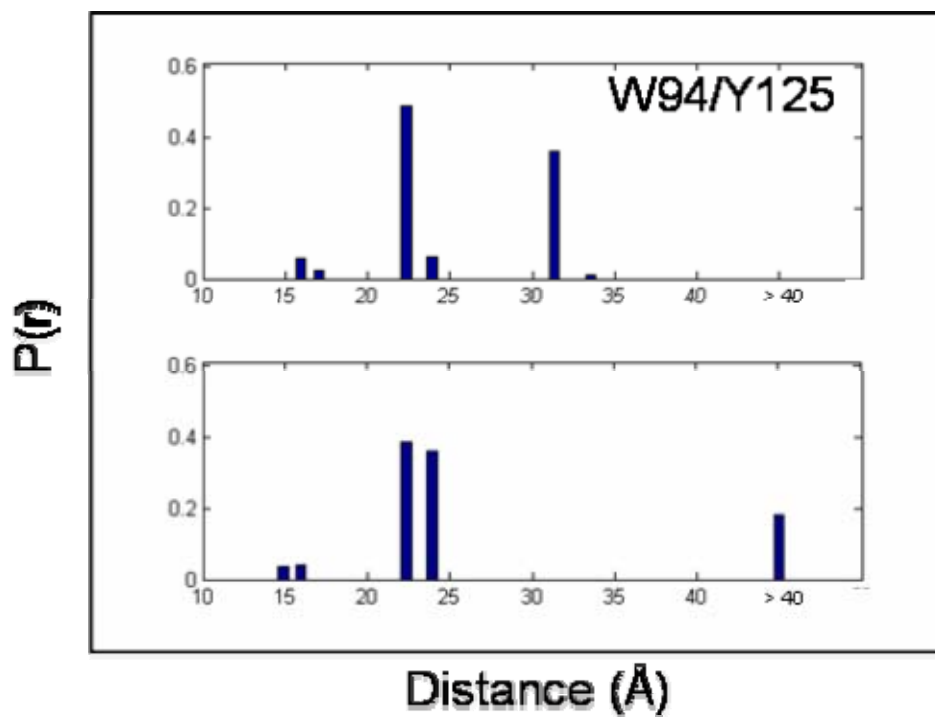


(a)

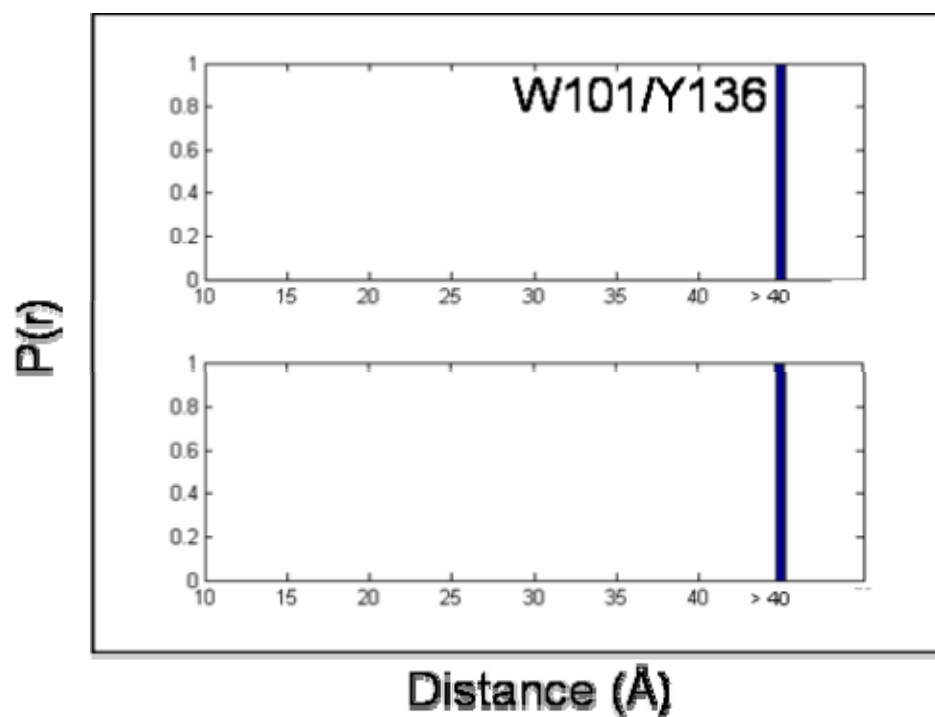


(b)

Figure 4.8. D-A distance distributions extrapolated from FET kinetics for (a) W125/Y136(NO_2) and (b) W94/Y136(NO_2) in 10 mM HEPES buffer (top panel), and 10 mM HEPES buffer with 1 mM Ca^{2+} (bottom panel)



(a)



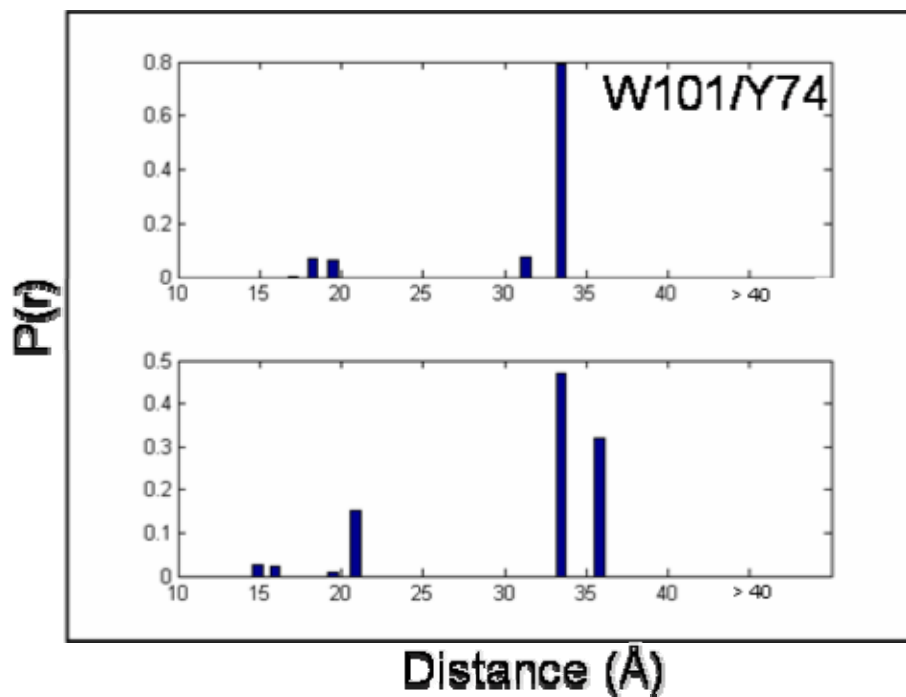
(b)

Figure 4.9. D-A distance distributions extrapolated from FET kinetics for (a) W94/Y125(NO_2) and (b) W101/Y136(NO_2) in 10 mM HEPES buffer (top panel), and 10 mM HEPES buffer with 1 mM Ca^{2+} (bottom panel)

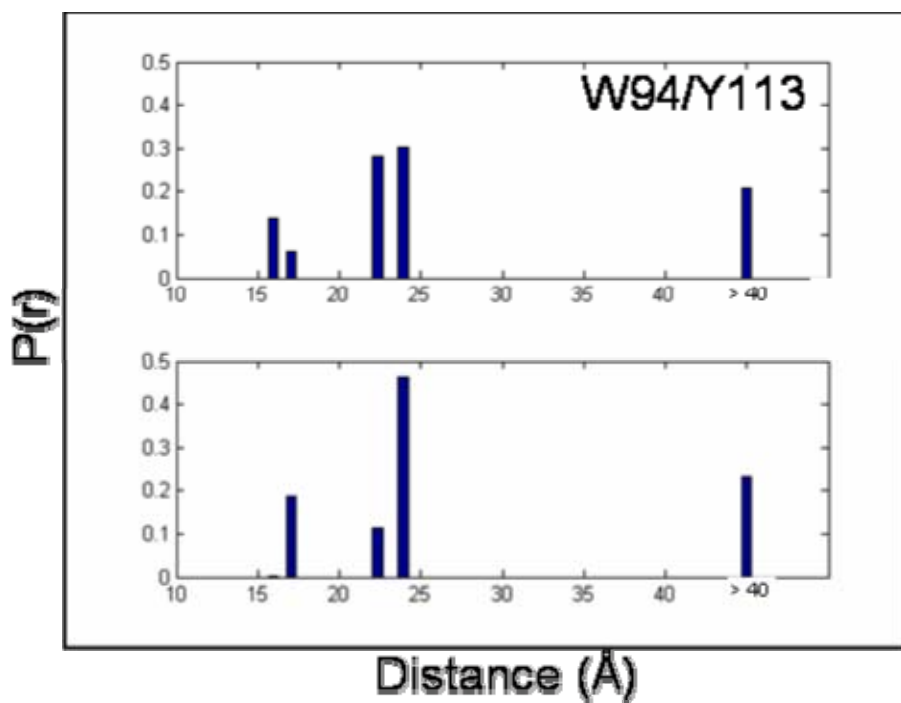
This pair, however, does not discount the possibility that there could be another calcium binding region in another part of the C-terminal tail. Following this hypothesis, we expect that the distance distributions for W101/Y136(NO₂) should decrease upon the addition of calcium ions. However, the D-A distances in both environments are still over the experimental limits of 40 Å.

On the other hand, in **Figure 4.10**, W101/Y74(NO₂) has a distribution of long (~ 33 Å, ~ 85%) and medium distances (18 Å, ~ 15%). However, upon the addition of calcium ions, the α -syn mutant sees a shift to slightly longer distances (~ 34 Å, 80%; ~ 20 Å, 15%). This suggests that this region experiences some lengthening when calcium ions are added. This slight lengthening phenomenon can also be observed for W94/Y113(NO₂) mutant, only to a much shorter extent. The population of extended distances (> 40 Å) remains largely the same (~ 20%), while there is a shift of the distance populations from ~ 22 Å to ~ 23 Å (60%) and from ~ 16 Å to ~ 17 Å (20%). Since the distance shift is much smaller for W94/Y113(NO₂) than W101/Y74(NO₂), it is possible that another calcium region can be found between residue 101 and 113, compensating for the lengthening between residue 74 and 101.

This binding region between residue 101 and 113 can be further proven by the distance distributions in W94/Y125(NO₂) as it gives an ensemble of extended distances (~ 32 Å, ~ 40%), intermediate distances (~ 23 Å, ~ 50%), and short distances (~ 16 Å, 10%). Adding calcium ions increases the intermediate distances' population significantly (75%). Similarly, for W101/Y125(NO₂) (**Figure 4.11**), a distance distribution of 38 Å to 36 Å (60%). It is interesting to note that the distance contraction for this D-A pair is very modest when compared to the one shown in the



(a)



(b)

Figure 4.10. D-A distance distributions extrapolated from FET kinetics for (a) W101/Y74(NO_2) and (b) W94/Y113(NO_2) in 10 mM HEPES buffer (top panel), and 10 mM HEPES buffer with 1 mM Ca^{2+} (bottom panel)

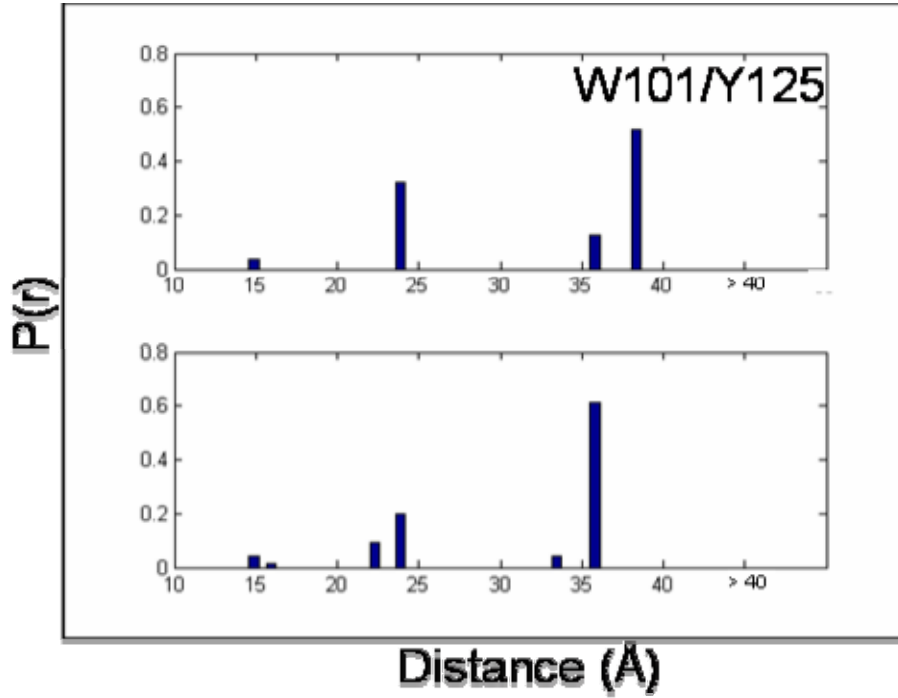


Figure 4.11. D-A distance distributions extrapolated from FET kinetics for W101/Y125(NO₂) in 10 mM HEPES buffer (top panel), and 10 mM HEPES buffer with 1 mM Ca²⁺ (bottom panel)

W125/Y136(NO₂) D-A pair. We can assign this phenomenon as an extending and rigidifying of the polypeptide between residues 113 and 125 upon the addition of calcium ions.

The C-terminal tail of α -syn behaves slightly differently when the mutants are in the presence of 1:1 POPC:POPA SUVs. For W101/Y74(NO₂) (**Figure 4.12**), the majority of the distance distribution slightly shifts from 33 Å to 31 Å upon the addition of calcium ions. A small population (10%) of short distance (19 Å) also emerges. Since this mutant belongs to part of the NAC region, it forms a helical structure in the presence of SUVs. Therefore, the slight decrease in distances is caused by a balance between the contraction due to helix formation and the lengthening between residues 94 and 101. This agrees with previous data as it is the region that has demonstrated association with the membrane when calcium ions and SUVs are present.

In **Figure 4.13**, for W101/Y125(NO₂), the distance distribution shifts from > 40 Å to 38 Å (~ 70%) when calcium ions were added. Similarly, W94/Y113(NO₂) shows a shift from > 40 Å to ~ 36 Å. These two D-A pairs show that some contraction is observed between residues 94 and 113. We have already concluded that there is a slight decrease in distances between residues 94 and 101. Therefore, there is a significant decrease of distances between residues 101 and 113. This region has already been identified as a calcium binding region in solution. This result reveals this calcium binding region is not affected when SUVs are present.

For W94/Y125(NO₂) (**Figure 4.14a**), there is a population of long polypeptide distance (> 40 Å, 40%) regardless of whether there are calcium ions present.

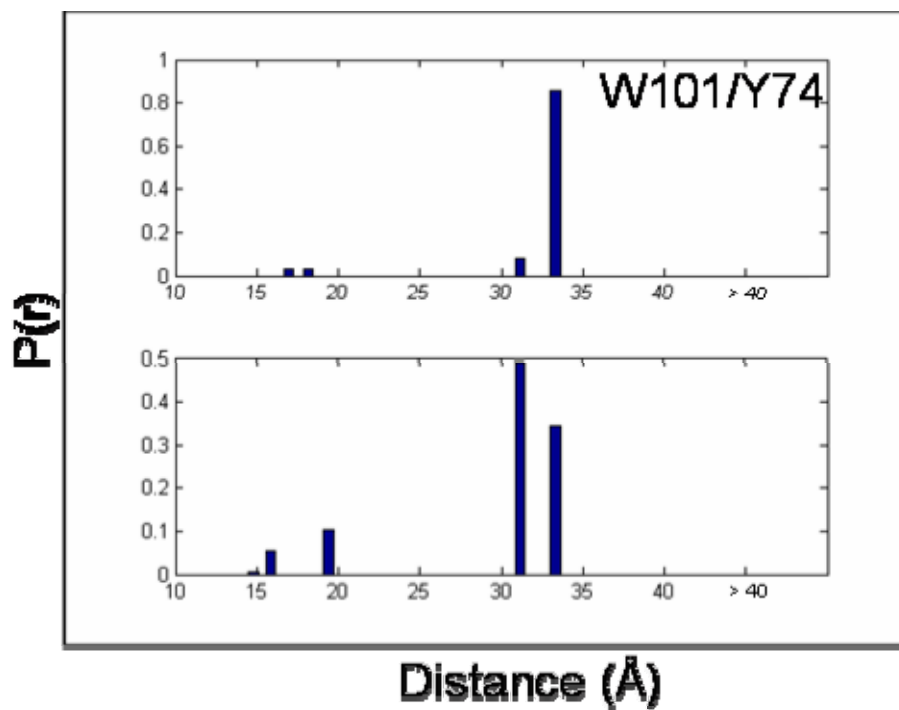
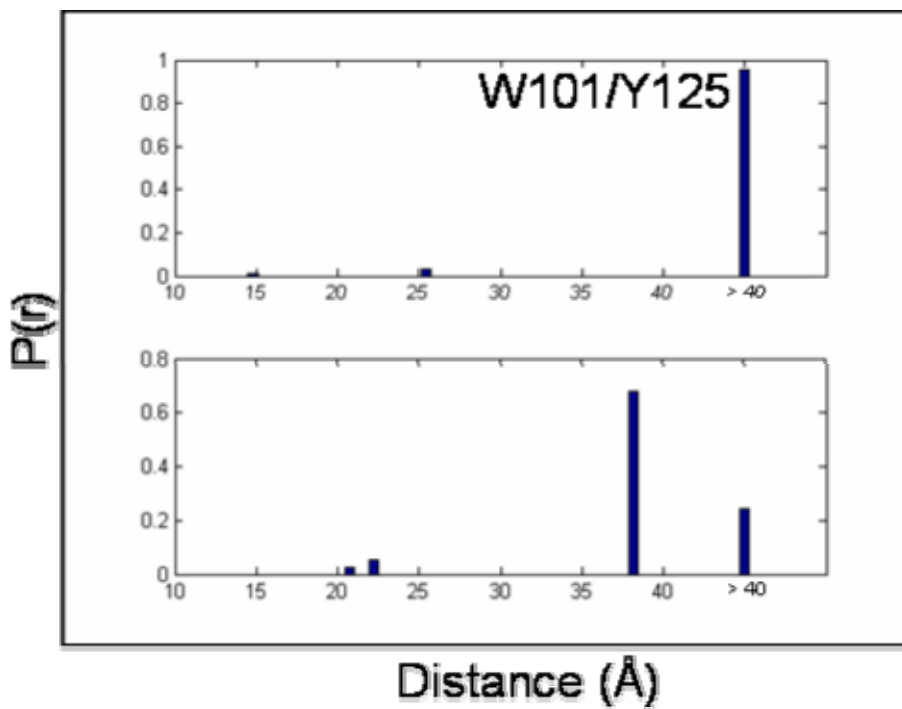
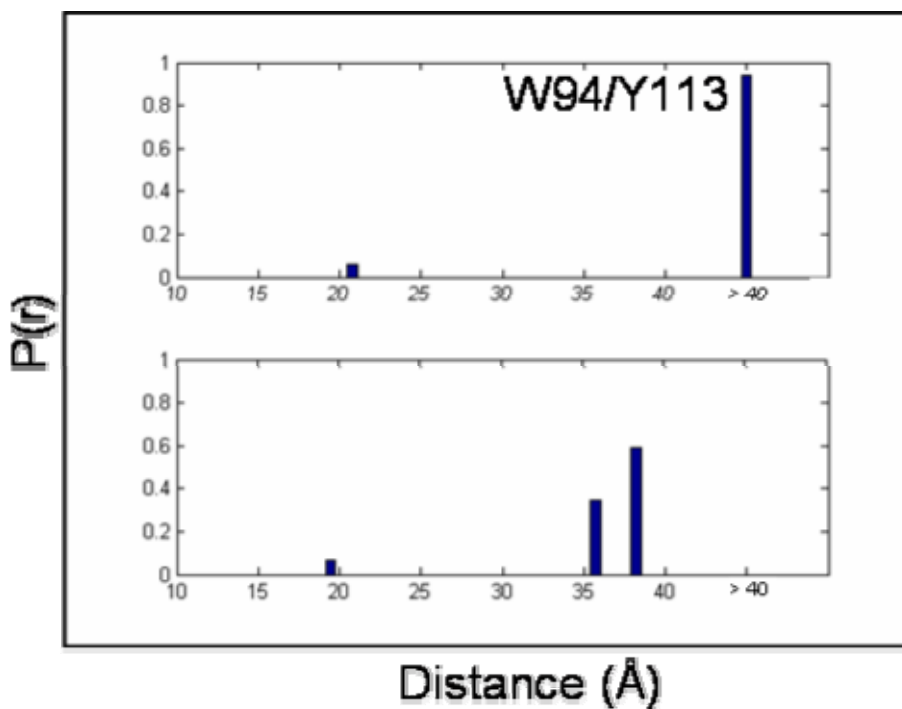


Figure 4.12. D-A distance distributions extrapolated from FET kinetics for W101/Y74(NO₂) in 1.4 mg/mL 1:1 POPC:POPA SUVs (top panel), and with 1 mM Ca²⁺ added (bottom panel)

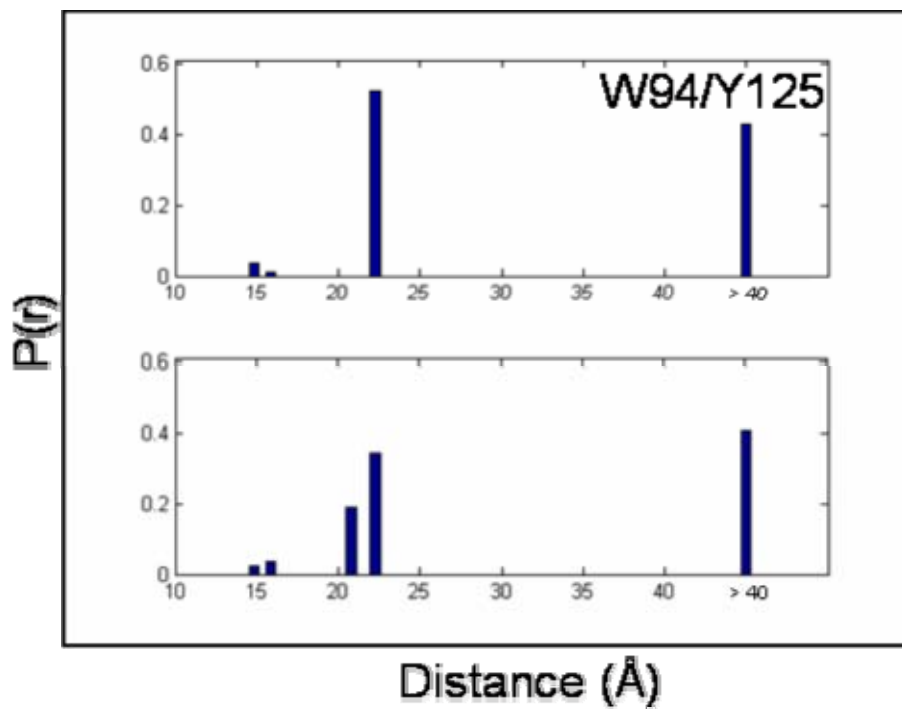


(a)

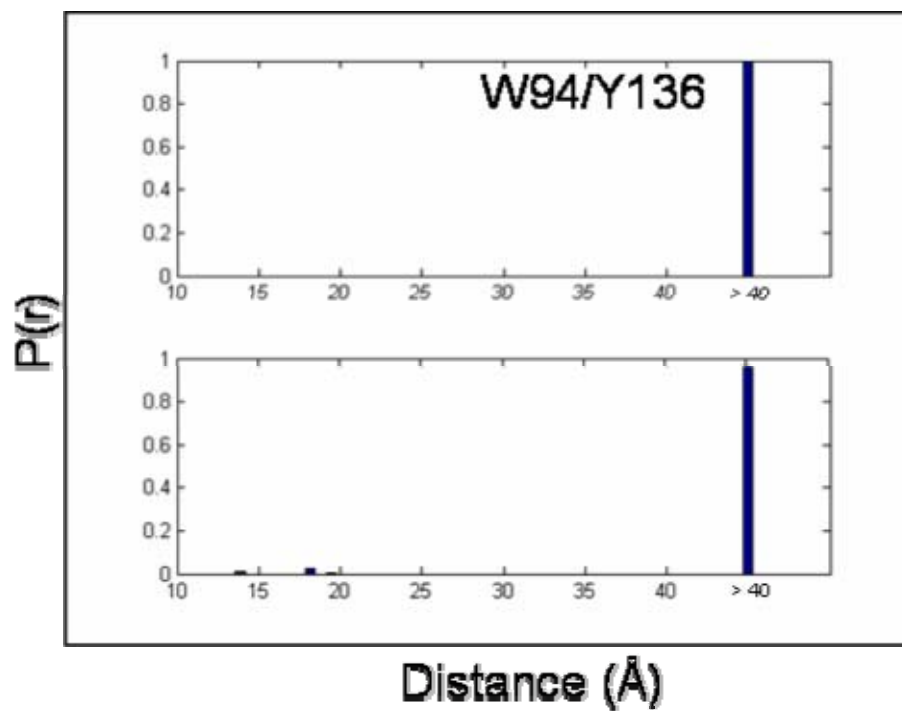


(b)

Figure 4.13. D-A distance distributions extrapolated from FET kinetics for (a) W101/Y125(NO_2) and (b) W94/Y113(NO_2) in 1.4 mg/mL 1:1 POPC:POPA SUVs (top panel), and with 1 mM Ca^{2+} added (bottom panel)



(a)



(b)

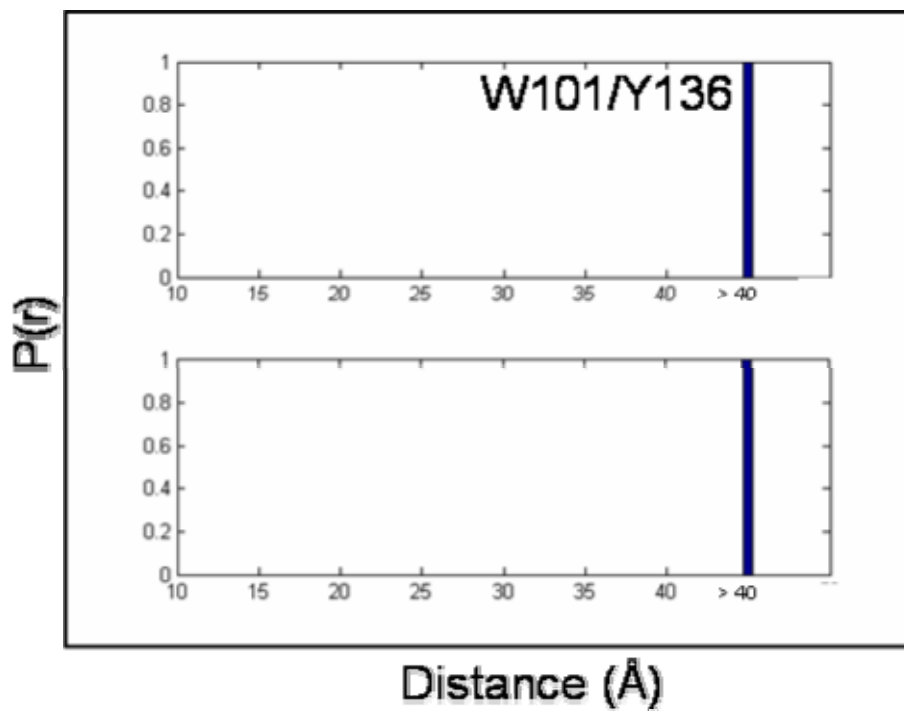
Figure 4.14. D-A distance distributions extrapolated from FET kinetics for (a) W94/Y125(NO_2) and (b) W94/Y136(NO_2) in 1.4 mg/mL 1:1 POPC:POPA SUVs (top panel), and with 1 mM Ca^{2+} added (bottom panel)

However, an intermediate polypeptide population (50%) shifts from 23 Å to 21 Å upon introducing calcium ions. This decrease of distances is much smaller than the one compared to W94/Y113(NO₂). Therefore, a lengthening site is required between residues 113 and 125 that will result in only a small decrease of distances in these two α -syn mutants.

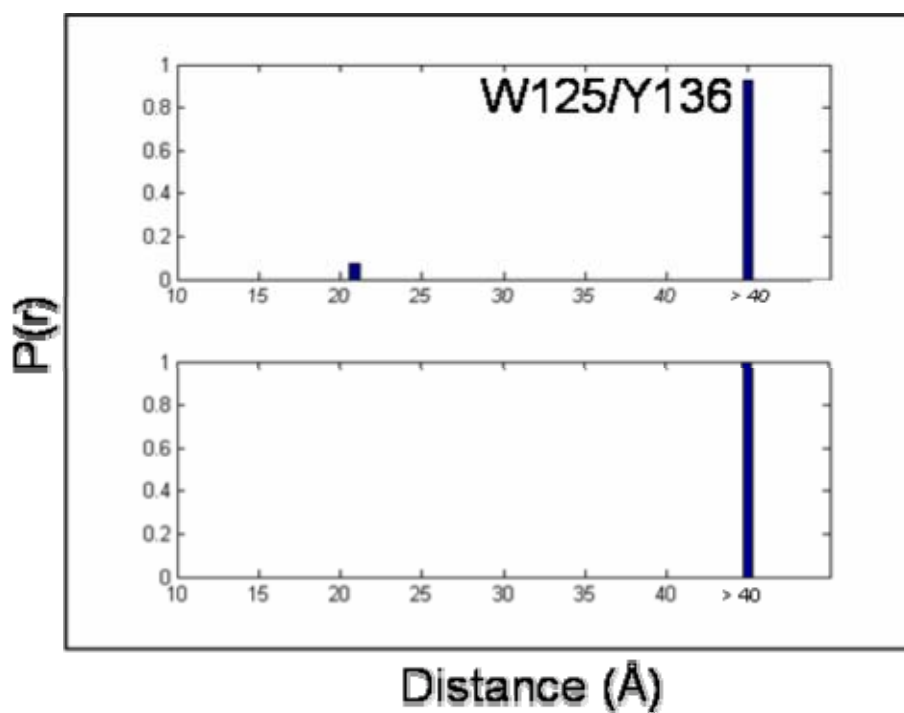
In **Figure 4.14b** and **Figure 4.15**, the time-resolved fluorescent energy transfer kinetics curves for W94/Y136(NO₂), W101/Y136(NO₂), and W125/Y136(NO₂) show that there is no quenching in these experiments (decay curves not shown), implying that the Trp and Tyr(NO₂) were too far apart for energy transfer to be effective. This could imply the disappearance or weakening of the calcium binding region between residue 125 and 136 in the presence of SUVs. The steric bulk of the associated SUV is one possible cause.

Circular Dichroism Studies.

Figure 4.16 shows the CD spectra of our seven C-terminal α -syn mutants in the buffer (red lines) and SUVs (black lines), in the presence (dotted lines) or absence (solid lines) of calcium ions. It has been suggested previously that α -syn mostly lacks structure in solution. The addition of calcium ions does not seem to induce any structural change to the mutants in solution. Also previously stated in Chapter 1, the presence of acidic SUVs can produce a highly helical structure. However, as demonstrated by **Figure 4.16**, no extra structures, such as β sheets, were introduced when calcium ions were introduced.



(a)



(b)

Figure 4.15. D-A distance distributions extrapolated from FET kinetics for (a) W101/Y136(NO₂) and (b) W125/Y136(NO₂) in 1.4 mg/mL 1:1 POPC:POPA SUVs (top panel), and with 1 mM Ca²⁺ added (bottom panel)

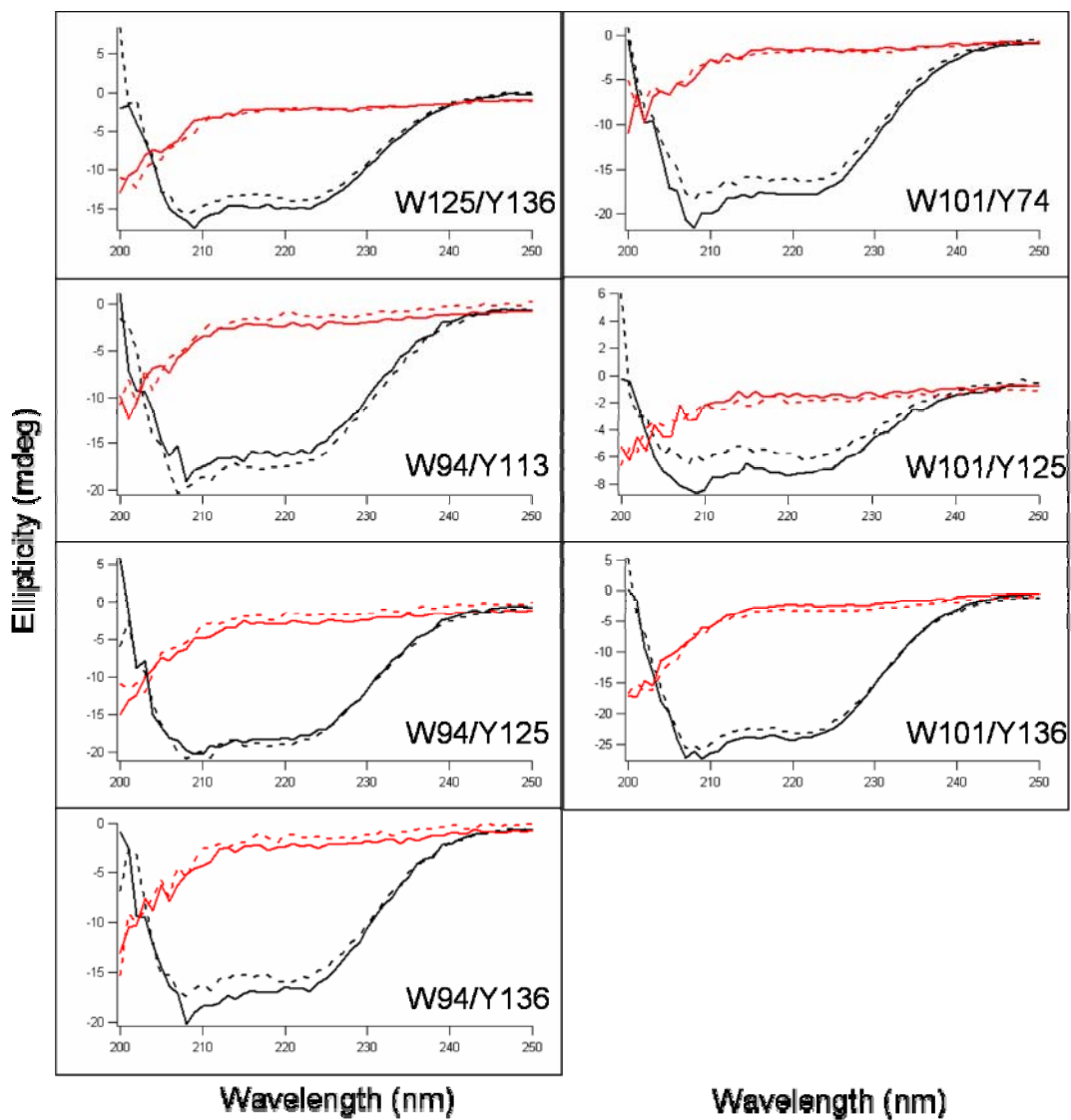


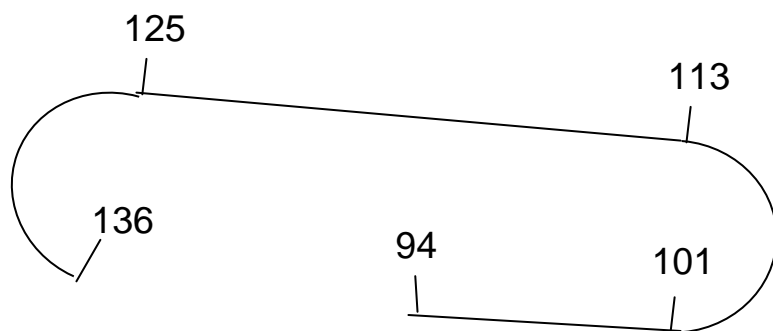
Figure 4.16. CD spectra of the seven C-terminal α -syn mutants in HEPES buffer (red solid line), HEPES + Ca^{2+} (red dotted line), 1:1 POPC:POPA SUVs (black solid line), and 1:1 POPC:POPA SUVs + Ca^{2+} (black dotted line)

Conclusion

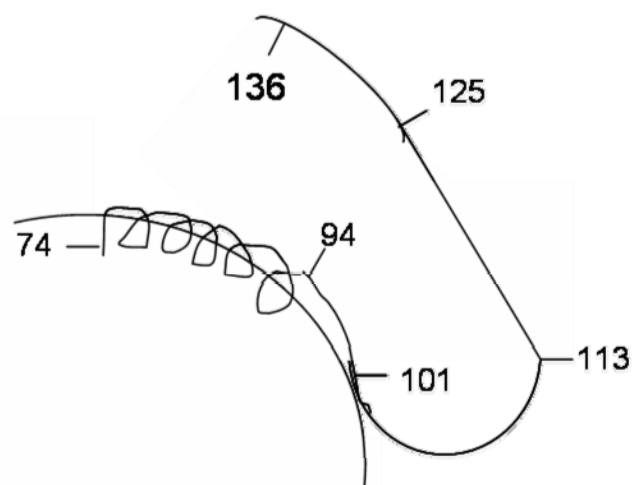
Using all the results collected from this study, **Figure 4.17** shows a pictorial description of the C-terminal tail structure in solution and SUVs in the presence of calcium ions. In this study, we have employed steady-state fluorescence spectroscopy on single Trp α -syn mutants in the C-terminal tail to investigate the amount of calcium ions needed to induce association with membrane. By incorporating quencher-containing lipids into SUVs, we have also deduced that the insertion of the C-terminal tail into the lipid bilayer is minimal. In addition, we have also conducted FET and contact quenching studies on seven α -syn mutants with Trp and Tyr(NO₂) incorporated as donor and acceptor.

Calcium binding has been observed for the amino acid sequence DX(D/N)XD.⁴⁶ **Figure 4.18** shows the sequence of the C-terminal tail of α -syn. Although this exact calcium binding motif is not present in the sequence, there are several regions which contain an acidic amino acid at positions one/five or one/three/five in the sequence.

Using that motif, we can identify the following potential calcium binding regions: residues 110–114, 115–119, 119–123, 126–130, 131–135, and 135–139. However, the several prolines (Pro117, Pro120, Pro128, Pro138) may disrupt the calcium binding capability of those polypeptides. By eliminating those possible calcium binding sites containing a proline in the sequence, the only possible binding regions that remain are residues 110–114 and 131–135. These two regions have been predicted to be the calcium binding sites experimentally.



(a)



(b)

Figure 4.17. A pictorial representation of the proposed C-terminal tail structure associated with calcium ions **(a)** in the absence of 1:1 POPC:POPA SUVs and **(b)** in the presence of 1:1 POPC:POPA SUVs

										80
Val	Thr	Gly	Val	Thr	Ala	Val	Ala	Gln	Lys	
										90
Thr	Val	Glu	Gly	Ala	Gly	Ser	Ile	Ala	Ala	
			94							100
Ala	Thr	Gly	Phe	Val	Lys	Lys	Asp	Gln	Leu	
101										110
Gly	Lys	Asn	Glu	Glu	Gly	Ala	Pro	Gln	Glu	
		113								120
Gly	Ile	Leu	Glu	Asp	Met	Pro	Val	Asp	Pro	
				125						130
Asp	Asn	Glu	Ala	Tyr	Glu	Met	Pro	Ser	Glu	
				136						140
Glu	Gly	Tyr	Gln	Asp	Tyr	Glu	Pro	Glu	Ala	

Figure 4.18. Amino acid sequence of the C-terminal tail of α -syn. The acidic residues (blue) and mutation sites (red) are highlighted

This study shows that the C-terminal tail of α -syn can bind to calcium ions. This binding process also induces some structural change to the protein. However, the binding mechanism of these calcium ions is still unclear. Therefore, future work will employ similar techniques to investigate whether this binding process is specific exclusively to calcium ions. First, we will look into the structural change of this C-terminal tail in an excess of protons (acidic environment). Second, we will study the effect of magnesium ions on the C-terminal tail structure as magnesium and calcium are similar in their electronic configurations.

4.5 ACKNOWLEDGEMENT.

This project was completed with the assistance of Ms. Stephanie S. E. Schulze and Mr. Matthew L. Robinson. Dr. Tetsunari Kimura also contributed in electron transfer experiment setup.

4.6 REFERENCES.

- (1) Clayton, D. F.; George, J. M. *Trends Neurosci.* **1998**, *21*, 249–254.
- (2) Lowe, R.; Pountney, D. L.; Jensen, P. H.; Gai, W. P.; Voelcker, N. H. *Protein Sci.* **2004**, *13*, 3245–3252.
- (3) Jensen, P. H.; Nielsen, M. S.; Jakes, R.; Dotti, G.; Goedert, M. *J. Biol. Chem.* **1998**, *273*, 26292–26294.
- (4) Nielsen, M. S.; Vorum, H.; Lindersson, E.; Jensen, P. H. *J. Biol. Chem.* **2001**, *276*, 22680–22684.
- (5) Jensen, P. H.; Islam, K.; Kenney, J.; Nielsen, M. S.; Power, J.; Gai, W. P. *J Biol Chem* **2000**, *275*, 21500–21507.
- (6) Fernandez, C. O.; Hoyer, W.; Zweckstetter, M.; Jares-Erijman, E. A.; Subramaniam, V.; Griesinger, C.; Jovin, T. M. *EMBO J.* **2004**, *23*, 2039–2046.
- (7) Park, S. M.; Jung, H. Y.; Chung, K. C.; Rhim, H.; Park, J. H.; Kim, J. *Biochemistry* **2002**, *41*, 4137–4146.
- (8) Kim, T. D.; Paik, S. R.; Yang, C. H.; Kim, J. *Protein Sci.* **2000**, *9*, 2489–2496.
- (9) Park, S. M.; Jung, H. Y.; Kim, T. D.; Park, J. H.; Yang, C. H.; Kim, J. *J. Biol. Chem.* **2002**, *277*, 28512–28520.

- (10) Souza, J. M.; Giasson, B. I.; Lee, V. M. Y.; Ischiropoulos, H. *Febs Letters* **2000**, *474*, 116–119.
- (11) Kim, T. D.; Paik, S. R.; Yang, C. H. *Biochemistry* **2002**, *41*, 13782–13790.
- (12) Serpell, L. C.; Berriman, J.; Jakes, R.; Goedert, M.; Crowther, R. A. *Proc. Natl. Acad. Sci.* **2000**, *97*, 4897–4902.
- (13) Crowther, R. A.; Jakes, R.; Spillantini, M. G.; Goedert, M. *Febs Letters* **1998**, *436*, 309–312.
- (14) Murray, I. V. J.; Giasson, B. I.; Quinn, S. M.; Koppaka, V.; Axelsen, P. H.; Ischiropoulos, H.; Trojanowski, J. Q.; Lee, V. M. Y. *Biochemistry* **2003**, *42*, 8530–8540.
- (15) Giasson, B. I.; Duda, J. E.; Murray, I. V. J.; Chen, Q. P.; Souza, J. M.; Hurtig, H. I.; Ischiropoulos, H.; Trojanowski, J. Q.; Lee, V. M. Y. *Science* **2000**, *290*, 985–989.
- (16) Fujiwara, H.; Hasegawa, M.; Dohmae, N.; Kawashima, A.; Masliah, E.; Goldberg, M. S.; Shen, J.; Takio, K.; Iwatsubo, T. *Nat. Cell Biol.* **2002**, *4*, 160–164.
- (17) Crowther, R. A.; Daniel, S. E.; Goedert, M. *Neurosci. Lett.* **2000**, *292*, 128–130.
- (18) Der-Sarkissian, A.; Jao, C. C.; Chen, J.; Langen, R. *J. Biol. Chem.* **2003**, *278*, 37530–37535.
- (19) Miake, H.; Mizusawa, H.; Iwatsubo, T.; Hasegawa, M. *J. Biol. Chem.* **2002**, *277*, 19213–19219.
- (20) Tamamizu-Kato, S.; Kosaraju, M. G.; Kato, H.; Raussens, V.; Ruyschaert, J. M.; Narayanaswami, V. *Biochemistry* **2006**, *45*, 10947–10956.
- (21) Ischiropoulos, H.; Beckman, J. S. *J. Clin. Invest.* **2003**, *111*, 163–169.
- (22) Denisova, N. A.; Strain, J. G.; Joseph, J. A. *J. Neurochem.* **1997**, *69*, 1259–1266.
- (23) Schulz, J. B.; Lindenau, J.; Seyfried, J.; Dichgans, J. *Eur. J. Biochem.* **2000**, *267*, 4904–4911.
- (24) Huang, C. L.; Huang, N. K.; Shyue, S. K.; Chern, Y. *J. Neurochem.* **2003**, *86*, 1247–1259.
- (25) Cuschieri, J.; Bulger, E.; Garcia, L.; Maier, R. V. *Surgery* **2005**, *138*, 158–164.
- (26) de Laureto, P.; Tosatto, L.; Frare, E.; Marin, O.; Uversky, V. N.; Fontana, A. *Biochemistry* **2006**, *45*, 11523–11531.
- (27) Lai, B. T.; Lee, J. C.; Gray, H. B.; Winkler, J. R. (Manuscript in preparation).
- (28) Forster, T. *Ann. Phys.-Berlin* **1948**, *2*, 55–75.
- (29) Lai, B. T.; Lee, J. C.; Gray, H. B.; Winkler, J. R. (Manuscript in preparation).
- (30) Lee, H. J.; Choi, C.; Lee, S. J. *J. Biol. Chem.* **2002**, *277*, 671–678.
- (31) Beechem, J. M.; Haas, E. *Biophys. J.* **1989**, *55*, 1225–1236.
- (32) Navon, A.; Ittah, V.; Landsman, P.; Scheraga, H. A.; Haas, E. *Biochemistry* **2001**, *40*, 105–118.
- (33) Lyubovitsky, J. G.; Gray, H. B.; Winkler, J. R. *J. Am. Chem. Soc.* **2002**, *124*, 14840–14841.
- (34) Wu, P. G.; Brand, L. *Anal. Biochem.* **1994**, *218*, 1–13.
- (35) Lee, J. C.; Gray, H. B.; Winkler, J. R. *J. Am. Chem. Soc.* **2005**, *127*, 16388–16389.

- (36) Lee, J. C.; Lai, B. T.; Kozak, J. J.; Gray, H. B.; Winkler, J. R. *J. Phys. Chem. B* **2007**, *111*, 2107–2112.
- (37) Jakes, R.; Spillantini, M. G.; Goedert, M. *Febs. Lett.* **1994**, *345*, 27–32.
- (38) Surrey, T.; Jahnig, F. *Proc. Natl. Acad. Sci. U. S. A.* **1992**, *89*, 7457–7461.
- (39) Reshetnyak, Y. K.; Koshevnik, Y.; Burstein, E. A. *Biophys. J.* **2001**, *81*, 1735–1758.
- (40) Kleinschmidt, J. H.; den Blaauwen, T.; Driessen, A. J. M.; Tamm, L. K. *Biochemistry* **1999**, *38*, 5006–5016.
- (41) Doring, K.; Konermann, L.; Surrey, T.; Jahnig, F. *Eur. Biophys. J.* **1995**, *23*, 423–432.
- (42) McIntosh, T. J.; Holloway, P. W. *Biochemistry* **1987**, *26*, 1783–1788.
- (43) Winkler, G. R.; Harkins, S. B.; Lee, J. C.; Gray, H. B. *J. Phys. Chem. B* **2006**, *110*, 7058–7061.
- (44) Arjara, G., California Institute of Technology, 2008.
- (45) Bolen, E. J.; Holloway, P. W. *Biochemistry* **1990**, *29*, 9638–9643.
- (46) Takada, Y.; Murphy, E.; Pil, P.; Chen, C.; Ginsberg, M. H.; Hemler, M. E. *J. Cell Biol.* **1991**, *115*, 257–266.